Supercritical CO2-induced atomistic lubrication for water flow in a rough hydrophilic nanochannel

Journal:	*Nanoscale*
Manuscript ID	NR-ART-08-2018-006204.R2
Article Type:	Paper
Date Submitted by the Author:	12-Oct-2018
Complete List of Authors:	Ho, Tuan; Sandia National Laboratories, Geochemistry Wang, Yifeng; Sandia National Laboratories Ilgen, Anastasia ; Sandia National Laboratories Criscenti, Louise; Sandia National Laboratories, Geochemistry Tenney, Craig; Sandia National Laboratories

SCHOLARONE™
Manuscripts

Supercritical CO_2-induced atomistic lubrication for water flow in a rough hydrophilic nanochannel

Tuan A. Ho[1]*, Yifeng Wang[2], Anastasia Ilgen[1], Louise J. Criscenti[1], and Craig M. Tenney[3]

[1] *Geochemistry Department, Sandia National Laboratories, Albuquerque, New Mexico 87185, USA.*

[2] *Nuclear Waste Disposal Research and Analysis Department, Sandia National Laboratories, Albuquerque, New Mexico 87185, USA.*

[3] *Nuclear Incident Response Program Department, Sandia National Laboratories, Albuquerque, New Mexico 87185, USA.*

Corresponding author:* taho@sandia.gov

Abstract:

A fluid flow in a nanochannel highly depends on the wettability of the channel surface to the fluid. The permeability of the fluid is usually very low, largely due to the adhesion of fluid at the solid interfaces. Using molecular dynamics (MD) simulations, we demonstrate that the permeability of water in a nanochannel with rough hydrophilic surfaces can be significantly enhanced by the presence of a thin layer of supercritical carbon dioxide ($scCO_2$) at the water-solid interfaces. The thin $scCO_2$ layer acts like an atomistic lubricant that transforms a hydrophilic interface into a super-hydrophobic one and triggers a transition from a stick- to- a slip boundary condition for a nanoscale flow. This work provides an atomistic insight into multicomponent interactions in nanochannels and illustrates that such interactions can be manipulated, if needed, to increase the throughput and energy efficiency of nanofluidic systems.

Introduction

Fluid slip along a fluid-solid interface is a fundamental topic in nanofluidics.[1-3] The degree of fluid slip is quantified by the slip length b, the distance extrapolated from the wall to where the flow velocity equals the wall velocity.[4] When b is much smaller than the channel height h (i.e., $b << h$), the slip can be ignored. This is true for most macroscopic flows for which a no-slip boundary condition is usually applied. Under nanoconfinement, the hydrodynamic slip can no longer be ignored, especially when $b \sim h$.[4] Large slip length is the main contributor for the massive flow enhancement in carbon nanotubes[5] and graphene nanopores.[6, 7]

Increasing fluid slip is often assumed to be associated with increasing surface hydrophobicity.[8-10] However, a few reports have suggested that slip can occur on hydrophilic surfaces[11, 12] and that water molecules can stick on hydrophobic substrates.[13] Manipulating surface properties and fluid-surface interactions to obtain a large slip is a matter of growing interest in science and technology, especially for practical applications including self-cleaning surface and energy conversion in nanofluidic devices.[14] Because of the correlation between surface hydrophobicity and hydrodynamic slip, super-hydrophobic surfaces (i.e., with a contact angle larger than 150^o) are usually designed to obtain large fluid flow enhancement. Such surfaces can be fabricated by engineering a shear-free air-liquid interface into a solid-liquid one using hydrophobic surface chemistry combining with micro- or nano-scale topological control of the solid surface.[4, 15, 16]

The question is whether it is possible to obtain a super-hydrophobic surface from an existing hydrophilic one without severely altering its chemistry or physical properties. A transition of a hydrophilic- to a hydrophobic surface may trigger a transformation from a stick- to- a slip boundary condition for a nanoscale flow. Here we present a MD simulation study to demonstrate the possibility for such a transition by exploiting the competitive adsorption of water and $scCO_2$ onto a rough nanochannel surface. We show that a thin layer of $scCO_2$ at a water-solid interface can act as an atomistic lubricant that can greatly facilitate a slipping fluid flow in a nanochannel. Our work points to a new mechanism and an engineering approach as well for increasing the throughput and reducing the energy consumption of nanofluidic systems in a wide range of energy-related or other applications.

Results and discussion

The MD simulations were performed on a water-kerogen system in the presence or absence of an accessory fluid or gas (i.e., $scCO_2$, N_2, or CH_4). Kerogen is a natural carbon material that provides a useful modeling system for understanding a potential effect of surface roughness and functional groups on a fluid flow in nanoconfinement.[17] In addition, kerogen is a major component in a shale gas/oil reservoir, and understanding fluid flows in kerogen nanopores is of great interest to gas/oil production from an unconventional reservoir.[17-19]

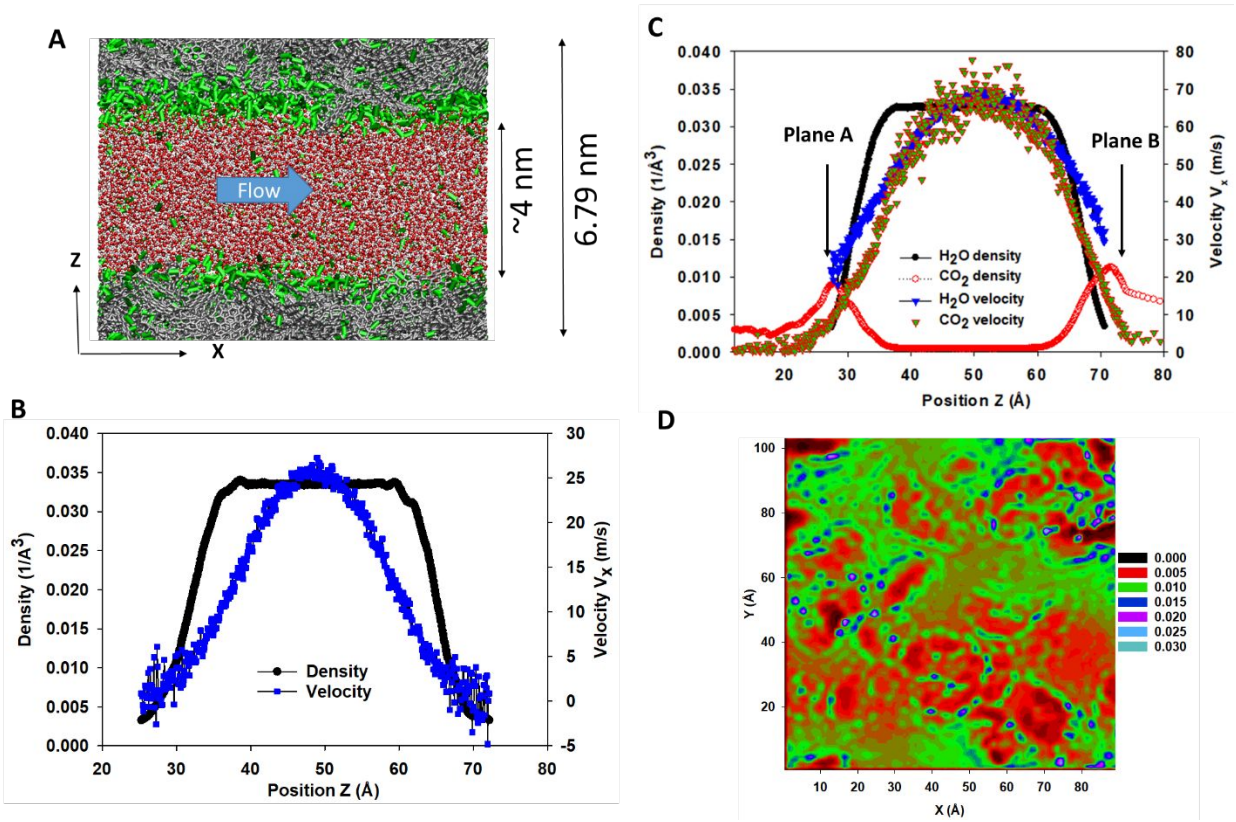

Figure 1. Simulation snapshot illustrating the flow of a water (red and white spheres) and CO_2 (green rods) mixture confined in kerogen nanopore (silver) (A). The size of the system without and with $scCO_2$ are 8.96×10.36×5.32 nm^3 and 8.96×10.36×6.79 nm^3, respectively. In the flow simulation, water molecules were forced to move in the x direction while the kerogen surface was kept stationary. Density and velocity profiles for pure water (B), and for the water and CO_2 mixture (C) confined in the kerogen nanopore obtained when water flow is fully established. Planes A and B in Fig. C mark top and bottom interfaces. Planar density distribution of CO_2 at top water-CO_2-kerogen interface (D). The color scale in Fig. D represents the density of CO_2 ($1/Å^3$).

In Fig. 1A we present a MD simulation snapshot to illustrate the geometry of a nanochannel used to study fluid flow in kerogen nanopores. It has been documented that significant amounts of water are found in kerogen nanopores, especially fine pores.[20, 21] In this study, we focus on the interaction of multicomponent fluids including CH_4, CO_2, N_2, and H_2O in kerogen nanopores. The kerogen surface in Fig. 1A was created from an over-mature kerogen molecule model shown in Fig. 2A. This realistic kerogen molecule model was designed to represent the chemistry of the kerogen found in the Duvernay shale.[22] In our previous work,[17-19] a periodic porous kerogen structure was

built to study both gas adsorption and transport, and the chemo-mechanical coupling between gas sorption and kerogen swelling. In this study, a different approach was employed to build a kerogen surface that is periodic in x and y directions, and non-periodic in z direction. The details of the method and the force field information used for the kerogen surface construction can be found in Supporting Information (SI). To construct the kerogen surface, we first built a kerogen/muscovite interface (Fig. 2B), representing an inorganic/organic interface analogous to those observed in SEM (Scanning Electron Microscope) images of shale samples.[23] The muscovite surface was then removed to create a kerogen-vacuum interface (Fig. 2C). The kerogen surface contains hydrophilic functional groups with oxygen, nitrogen, and sulfur atoms, and hydrophobic hydrocarbon groups as well.[22] The result reported in Fig. 2D also suggests that a kerogen surface is rough at an atomistic level. This rough surface is probably a better representation of many actual nanofluidic systems, and the effect of surface roughness on fluid flows is an interesting topic for nanofluidics research.[24, 25] Note that the constrained parameter used to build the kerogen surface is the density of the kerogen slab (see SI for more details). There is no control on the surface roughness in the simulation to construct the kerogen surface.

In our simulations, the water flow was driven in the x direction by an acceleration of 3×10^{-4} Kcal/Å.g (i.e., $\sim12.55\times10^{12}$ m/s^2) applied to all water molecules present in the kerogen nanochannel as shown in Fig. 1A (i.e., Poiseuille flow, see SI for more details). The presence or absence of hydrodynamic slip can be studied when a steady state is reached. The temperature was set at 300 K. The pressure in the z direction was 200 atm, which is typical for a shale gas/oil reservoir or geological storage of CO_2. Comparing the velocity profiles of water in the system with and without $scCO_2$ reveals the effect of $scCO_2$ on the water flow in kerogen nanochannels. In Fig. 1B, we report the density and velocity profiles of pure water in the kerogen nanopore (i.e., the system without $scCO_2$). Water-kerogen interface was defined to be the regions where the water density equals 10% of the bulk water density. The density profile indicates that the water density reaches bulk density (~0.033 molecules/Å^3 or ~1 mg/l) at the pore center and gradually reduces toward the kerogen surfaces. Because of the surface roughness, we do not observe multiple interfacial water layers on the kerogen surface as we observe in the 1D density profile for water on a flat surface.[11] The velocity profile of water in the nanochannel (Fig. 1B) indicates that at the water-kerogen interface, the water molecules have a zero velocity (with minor fluctuations around

zero due to thermal noises). Therefore, the water flow in the kerogen nanochannel exhibits a no-slip boundary condition.

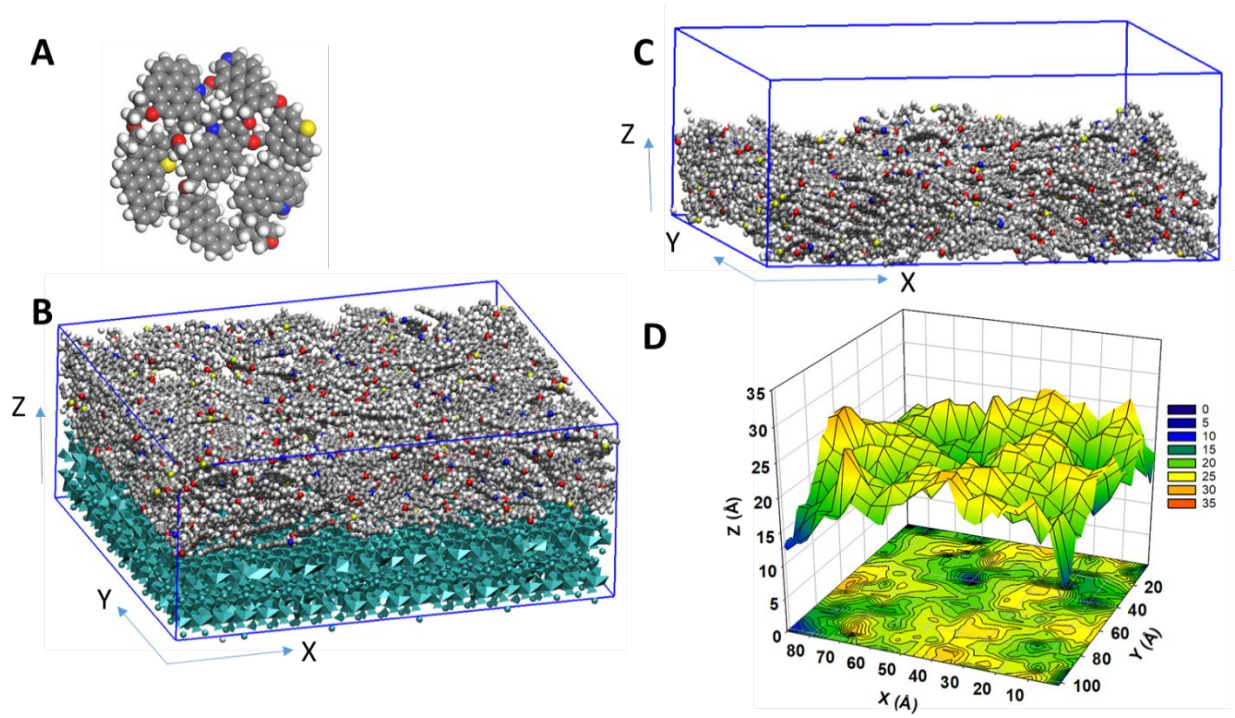

Figure 2. Model kerogen molecule used in this work (A). Note that the color code for kerogen atoms is different from that for kerogen atoms in Fig. 1. Silver, red, blue, yellow, and white spheres represent carbon, oxygen, nitrogen, sulfur, and hydrogen, respectively. Simulation snapshot demonstrates the kerogen/muscovite (cyan) (B) and kerogen/vacuum (C) interfaces. The altitude z of the uppermost kerogen atoms as a function of x and y (D). The contour plot in xy plane is the projection of the z coordinates. The color scale in Fig. D represents the z coordinates.

The no-slip boundary condition observed for water flow in the kerogen nanochannel is consistent with the contact angle result presented in Fig. 3A. A water droplet of 1100 water molecules was placed on the kerogen surface and equilibrated using an NVT ensemble [constant number of atoms, volume, and temperature (300K)]. The contact angle of $42.8^{o}\pm6.5^{o}$ (see SI for more details about contact angle and error calculations) suggests that a kerogen surface is hydrophilic. Interestingly, when adding $scCO_2$ at 200 atm into the system of Fig. 3A (see SI) the partially water-wetting kerogen-water interface transforms into a non-water-wetting interface (i.e., with a contact angle of 180^{o}, Fig. 3B). This transition is reversible because when we remove all the CO_2 molecules, the water droplet in Fig. 3B converts back to the droplet in Fig. 3A. The dynamics of the transition

from a small contact angle water droplet into a spherical droplet is of great interest for both fundamental understanding and practical applications, for example, for the development of smart self-cleaning surfaces and more robust coating agents.[26] The transition from a hydrophilic to hydrophobic kerogen interface when adding $scCO_2$ is in good agreement with experimental data that the contact angle of water on mineral surfaces increases with increasing CO_2 pressure.[27, 28]

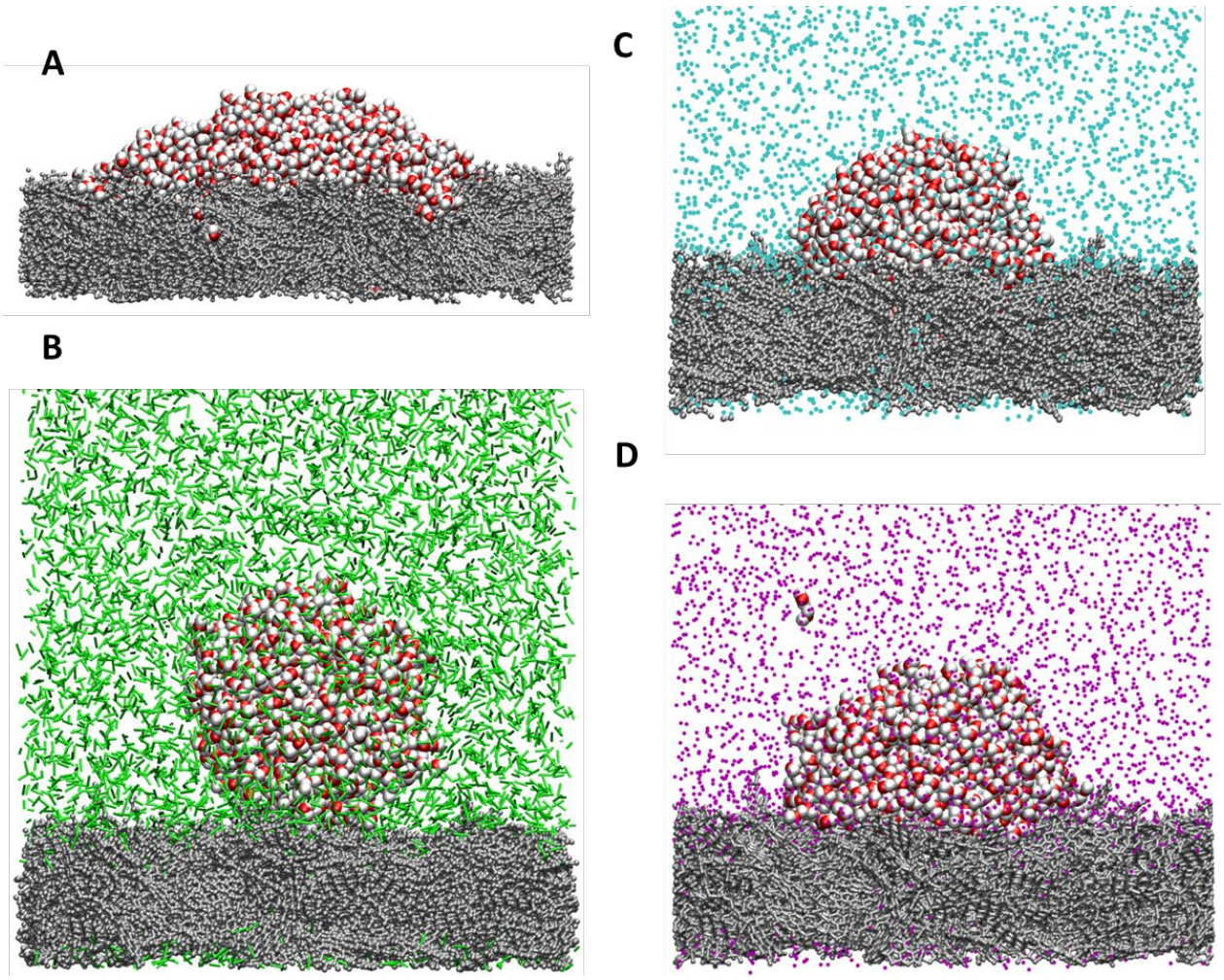

Figure 3. Simulation snapshots illustrating the final configurations of 1100 water molecules droplets in vacuum (A), in 200atm CO_2 (B), N_2 (C), and CH_4 (D) on a kerogen surface. Water molecules are shown in red and white. Kerogen atoms are all colored as silver. CO_2, N_2 and CH_4 are exhibited in green, cyan, and purple, respectively. See SI for force field information and simulation conditions.

When $scCO_2$ is replaced by N_2 or CH_4 at the same gas pressure (200 atm), the contact angle increases compared to that of water in air (or vacuum). The contact angle of water in 200 atm N_2 (Fig. 3C) or CH_4 (Fig. 3D) is $63.52^o \pm 0.21^o$ or $79.18^o \pm 1.97^o$, respectively. However, the contact angle is still smaller than 90^o, indicating that the kerogen surface remains hydrophilic in N_2 or CH_4 atmosphere. The competitive adsorption of the $scCO_2$ over water onto the kerogen surface is the key factor for the transformation of a partially water-wetting into a non-water-wetting interface. In our previous work[19] we show that kerogen has higher affinity for the adsorption of CO_2, compared to CH_4 and N_2. For this reason, the contact angle of water droplet in $scCO_2$ is larger than that of water droplet in CH_4 and N_2 at the same gas pressure.

The dewetting of a small contact angle droplet into a spherical drop by adding $scCO_2$ presented in Fig. 3 has interesting consequence regarding the water flow in nanochannel. In Fig. 1C, we show both water and $scCO_2$ densities and velocities within the kerogen nanochannel. The water concentration is the same as in Fig. 1B. The CO_2 molecules were introduced in the middle of the pore (see SI) at the beginning of the simulation with a CO_2/water ratio of ~0.19 (2100 CO_2 and 10950 H_2O molecules). The pressure and temperature are the same as those used for the system in Fig. 1B (T = 300 K, P = 200 atm). At equilibrium, some CO_2 molecules adsorb inside the kerogen structure, and some CO_2 molecules dissolve into the water. However, the focus of this discussion is the CO_2 layer formed at the water-kerogen interface (i.e., 10Å CO_2 layers centered at planes A and B in the density profile in Fig. 1C, more details of the configuration of the CO_2 layer with respect to kerogen atoms is provided in the SI). These CO_2 layers form because of the competitive adsorption of CO_2 over H_2O onto kerogen surfaces, which will be explained later.

The velocity profile of CO_2 indicates that CO_2 flow exhibits a no-slip boundary condition at kerogen/CO_2 interface. At CO_2/water interface, water flows faster than CO_2 (i.e., at planes A and B in Fig. 1C, note that there is no external force applied on CO_2 molecules, CO_2 molecules move in the x direction is because of the interaction with water). Therefore, water slips on CO_2 layers. The velocities of water at planes A and B in Fig. 1C are 22 m/s and 32 m/s, respectively. From the slip velocity one can estimate the friction coefficient λ using $\lambda = \frac{F_f}{2Av_s}$ where F_f is the friction force (force parallel to the flow direction), v_s is the slip velocity, A is the surface area, and factor '*2*' is for two interfaces in our simulation box.[3, 29, 30] The friction force equals the total external force acting on all water molecules (i.e., 59.13 Kcal/mol.Å). For the flow with CO_2 layers, the friction

coefficients are ~100x10^4 and ~69x10^4 Ns/m^3 at planes A and B, respectively. For the case of no-slip boundary condition of water flow without CO_2, (i.e., zero slip velocity v_s=0) one can estimate the friction coefficient from the equilibrium data (i.e., obtained from equilibrium simulation without external force) using the Green-Kubo relation, which is beyond the scope of this work.[3, 31] In addition, the calculated slip lengths at planes A and B are 8.56±1.00Å and 15.81±4.28Å, respectively (see SI for more details). The differences in the slip velocity and slip length at planes A and B are due to the fact that the kerogen interfaces at planes A and B are not the same and the amount of CO_2 accumulated at planes A and B is different (see the CO_2 density profile). The finite velocities at planes A and B strongly indicate that water flow in the kerogen nanochannel in the presence of scCO_2 exhibits hydrodynamic slip, which is substantially different from the no-slip water flow observed in Fig. 1B.

Because of the slip effect the water flow rate for the system with scCO_2 is ~4 times higher than that for the system without scCO_2 (i.e., enhancement factor of 4, comparing on the basis of the same amount of water molecules in the kerogen nanochannel). The result thus demonstrates the capability of an interfacial scCO_2 layer acting as an atomistic lubricant in enhancing water flow in a nanochannel with rough hydrophilic surfaces. This idea is in some sense similar to the existing approach to engineering a shear-free air-liquid interface into a solid-liquid interface by introducing nanometer to micrometer-scale roughness onto a solid surface,[32] but here a gas-liquid interface is introduced at a much smaller scale (at a molecular scale). We believe that surface roughness is not necessary for the enhanced permeability. The preferential adsorption of scCO_2 over water onto a smooth surface would enhance the flow rate of water as well. In Fig. 1D we show the surface density distribution of scCO_2 on the xy plane (i.e., density map). The CO_2 molecules within the 10Å layer centered at the plane B were considered in this calculation. The density map indicates that CO_2 molecules spread all over the kerogen surfaces; however, the molecules are not evenly distributed because of the surface roughness. This illustrates the effectiveness of scCO_2 to intercalate between water and kerogen surfaces to form a new kerogen-scCO_2-water interface.

In our work, the simulation box is periodic in the flow direction. Some CO_2 molecules in the middle of the pore and in the layers at planes A and B leave the channel at one end and enter the channel at the other end (see CO_2 velocity profile in Fig. 1C). The CO_2 density profile indicates that CO_2 layers remain in between water and kerogen during flow simulation. In reality, the

channel is usually short and has two ends. To maintain the lubricant effect for water flow, we may need to introduce additional CO_2 with water at the entrance.

To provide more details about (1) the competitive adsorption of CO_2 over H_2O onto a kerogen surface leading to the formation of a stable CO_2 layer between H_2O and kerogen as shown in Fig. 1 and (2) the larger contact angle of water droplet in CO_2 environment compared to that of water droplet in CH_4 atmosphere shown in Fig. 3, we conducted additional simulations to analyze the interaction energy of CO_2, CH_4, and H_2O with kerogen. In these simulations 2462 of pure CO_2, CH_4, or H_2O molecules were placed in the simulation box of 89.67x103.66x100 $Å^3$ with a kerogen surface present. The simulations were carried out for 3ns in the NVT ensemble. The total pair interaction energy (i.e., that of 2462 molecules with kerogen including the Lennard-Jones (LJ) and electrostatic (Coulomb) interactions) reported in Fig. 4A indicates that CO_2 interacts with kerogen stronger, compared to H_2O. The interaction of CO_2 with kerogen was decomposed into the LJ and electrostatic interactions (Fig. 4B, red and blue lines), and the result suggests that the LJ interaction is much larger than the electrostatic interaction. Further analysis of the LJ interaction of CO_2 with kerogen indicates that LJ interaction from 2 oxygen atoms of CO_2 with kerogen (Fig. 4B, purple line) plays an important role in the CO_2 interaction with kerogen surface. Similarly, for water (Fig.4C), the LJ interaction with kerogen is stronger than the electrostatic interaction. Note that the electrostatic interaction of water with kerogen is stronger compared to that of CO_2 with kerogen (red lines in Fig. 4B and 4C), which is expected due to the strong dipole moment of water compared to the zero external dipole moment of CO_2.[28, 33] However, the LJ interaction of CO_2 with kerogen is sufficiently strong, compared to that of water leading to formation of stable CO_2 layers between kerogen and H_2O. In addition, the molecular model of kerogen presented in Fig. 2A indicates that the over mature kerogen is composed of large segments of the aromatic hydrocarbons, which is similar to the structure of graphene. On the perfect graphene surface the selectivity of CO_2 over water is ~7.2.[33]

The comparison of the interaction energy of CO_2 and CH_4 with kerogen presented in Fig. 4A explains the larger contact angle of water on kerogen surface in CO_2 atmosphere, compared to that of water on kerogen surface in CH_4 atmosphere (as presented in Fig 3). Contact angle θ of water can be calculated using Young's equation:

$$Cos\theta = \frac{\gamma_{s/g} - \gamma_{s/w}}{\gamma_{g/w}} \quad (1)$$

Where γ is the surface tension and *s*, *g*, and *w* are for solid, gas, and water, respectively. Our results indicate that contact angle of water in CO_2 is greater than that of water in CH_4 environment:

$$Cos\theta_{w/CO_2} < Cos\theta_{w/CH_4} \quad (2)$$

Combining (1) and (2) we have

$$\frac{\gamma_{s/CO_2} - \gamma_{s/w}}{\gamma_{CO_2/w}} < \frac{\gamma_{s/CH_4} - \gamma_{s/w}}{\gamma_{CH_4/w}} \quad (3)$$

In our simulation, solid phase (i.e., kerogen) and water are the same in CO_2 and CH_4 environments, therefore $\gamma_{s/w}$ is constant. Because $\gamma_{CO_2/w} < \gamma_{CH_4/w}$[34-36] inequality (3) is true when $\gamma_{s/CO_2} \ll \gamma_{s/CH_4}$. To the best of our knowledge, there is no reported interfacial tension of kerogen with CO_2 and CH_4 available in the literature. However, the comparison of the interaction energy of CO_2 and CH_4 with kerogen reported in Fig. 4A indicates that CO_2 interacts more strongly with kerogen compared to CH_4. In addition, in our previous work[19] kerogen preferentially adsorbs CO_2 over CH_4. Therefore, we postulate that $\gamma_{s/CO_2} \ll \gamma_{s/CH_4}$.

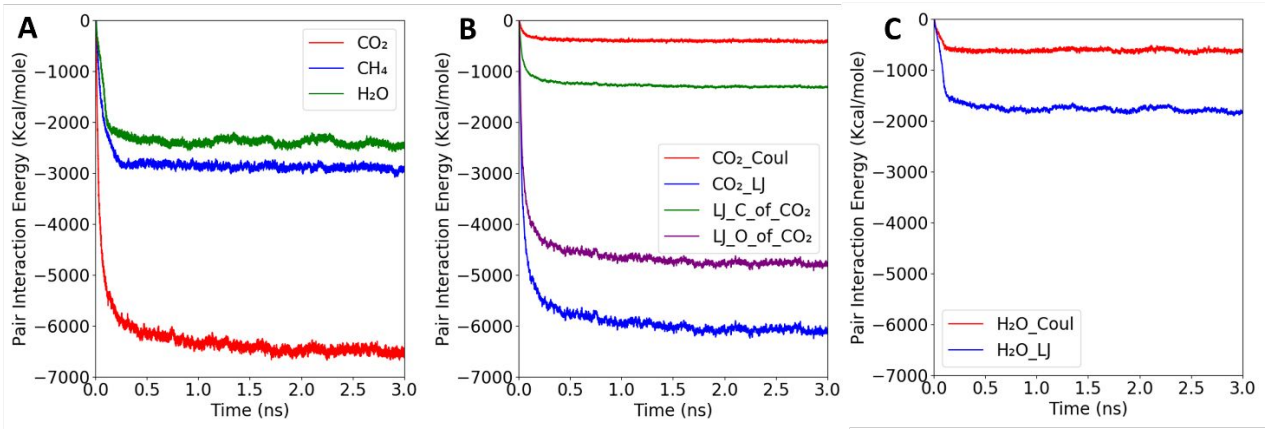

Figure 4. Pair interaction energy of CO_2 (red), CH_4 (blue), and H_2O (green) molecules with kerogen (A). Eelectrostatic (red) and LJ (blue) interactions of CO_2 molecules with kerogen, and the LJ interactions of the carbon (green) and oxygen (purple) atoms of CO_2 molecule with kerogen (B). Electrostatic (red) and LJ (blue) interaction energy of water with kerogen (C).

Recent experimental and modeling studies have illustrated that with decreasing nanopore size, the thermodynamic properties of water are altered. A decrease in the dielectric constant by 50% was

reported for 1.2 nm pore.[37, 38]A decrease in density and surface tension was also reported for confined water, compared to the bulk phase.[39] These changes in water properties are due to the distortion in hydrogen-bonding networks, with increasing hydrogen-bonding and increasing fraction of 4-coordinated waters with decreasing pore size.[40, 41] The pore diameter modeled in our study was ~4 nm, which is at the scale where a nanoconfinement effect may become pronounced. Given the earlier observations and our results, we hypothesize that with decreasing pore size and decreasing water density, the effect of the atomistic lubricant will be increasing. We do not anticipate any significant nanoconfinement effect for $scCO_2$, in comparison to H_2O, since CO_2 molecules lack adipole moment.

The wettability of kerogen under the different conditions presented in Fig. 3 is critical for understanding the fate of aqueous hydraulic fracturing fluids, CO_2, and CH_4 in shale reservoirs and in shale caprock during geological carbon storage.[42] Traditional wisdom is that the shale organic pore is hydrophobic.[42] However, our results show that kerogen is partially water-wetting (Fig. 3A, C, and D) due to its hydrophilic functional groups and surface roughness. This conclusion is consistent with the fact that water has been experimentally found in organic nanopores, especially with decreasing pore size.[20, 21] In addition, the result shown in Fig. 3B indicates that kerogen is CO_2-wetting and that CO_2 can expel water from kerogen interfaces. These conclusions together with our previous result show that CO_2 can displace large amount of CH_4 in kerogen nanopores[19] indicate that kerogen could provide an effective sink for CO_2 during geological storage. We also want to postulate that the lubrication mechanism demonstrated above may have an implication to the release of produced water in an unconventional oil/gas reservoir, an interesting topic certainly worth further research. In addition, a large contact angle of water droplet in $scCO_2$ environment was also observed on siloxane surface of kaolinite, and a CO_2 layer was also found between kaolinite and water droplet.[43] This can serve as an indirect piece of evidence that CO_2 can sandwich not only between kerogen and water, but also between mineral and water.

Conclusions

In summary, using molecular dynamics simulations of water flow in a realistic kerogen nanochannel, we have demonstrated that a stick to slip transition of a water flow in a nanochannel can be induced by incorporating an accessory fluid component (e.g., $scCO_2$), which has a limited solubility in water and, through competitive adsorption, can spontaneously form an atomistically

thin layer over a rough hydrophilic surface and therefore lubricate the water in the nanochannel. Once verified experimentally, this result can provide a new engineering approach to obtain a hydrophobic or super-hydrophobic interface from an existing hydrophilic one without significantly alteration in surface topology. This could lead to the technological advancement for a variety of applications including water desalination and energy conversion in nanofluidic devices.

Conflicts of interest

There are no conflicts to declare.

Acknowledgements

Sandia National Laboratories is a multi-mission laboratory managed and operated by National Technology and Engineering Solutions of Sandia, LLC., a wholly owned subsidiary of Honeywell International, Inc., for the U.S. Department of Energy's National Nuclear Security Administration under contract DE-NA0003525. The views expressed in this article do not necessarily represent the views of the U.S. Department of Energy or the United States Government. This research was funded by a DOE National Energy Technology Laboratory project (to Y. Wang) and by the Center for Frontiers in Subsurface Energy Security, an Energy Frontier Research Center funded by the U.S. Department of Energy, Office of Science, Office of Basic Energy Sciences under Award Number DE-SC0001114.

References

1. I. U. Vakarelski, E. Klaseboer, A. Jetly, M. M. Mansoor, A. A. Aguirre-Pablo, D. Y. C. Chan and S. T. Thoroddsen, *Sci Adv*, 2017, **3**, e1701558.
2. J. C. T. Eijkel and A. van den Berg, *Microfluid. Nanofluid.*, 2005, **1**, 249-267.
3. G. Tocci, L. Joly and A. Michaelides, *Nano Lett.*, 2014, **14**, 6872-6877.
4. R. S. Voronov, D. V. Papavassiliou and L. L. Lee, *Ind Eng Chem Res*, 2008, **47**, 2455-2477.
5. J. K. Holt, H. G. Park, Y. M. Wang, M. Stadermann, A. B. Artyukhin, C. P. Grigoropoulos, A. Noy and O. Bakajin, *Science*, 2006, **312**, 1034-1037.
6. B. Radha, A. Esfandiar, F. C. Wang, A. P. Rooney, K. Gopinadhan, A. Keerthi, A. Mishchenko, A. Janardanan, P. Blake, L. Fumagalli, M. Lozada-Hidalgo, S. Garaj, S. J. Haigh, I. V. Grigorieva, H. A. Wu and A. K. Geim, *Nature*, 2016, **538**, 222-225.
7. R. R. Nair, H. A. Wu, P. N. Jayaram, I. V. Grigorieva and A. K. Geim, *Science*, 2012, **335**, 442-444.
8. D. Ortiz-Young, H. C. Chiu, S. Kim, K. Voitchovsky and E. Riedo, *Nat Commun*, 2013, **4**, 2482
9. K. L. Wu, Z. X. Chen, J. Li, X. F. Li, J. Z. Xu and X. H. Dong, *Proc. Natl. Acad. Sci. U.S.A.*, 2017, **114**, 3358-3363.
10. D. M. Huang, C. Sendner, D. Horinek, R. R. Netz and L. Bocquet, *Phys. Rev. Lett.*, 2008, **101**, 226101
11. T. A. Ho, D. V. Papavassiliou, L. L. Lee and A. Striolo, *Proc. Natl. Acad. Sci. U.S.A.*, 2011, **108**, 16170-16175.

12. K. P. Lee, H. Leese and D. Mattia, *Nanoscale*, 2012, **4**, 2621-2627.
13. C. Bakli and S. Chakraborty, *Nano Lett.*, 2015, **15**, 7497-7502.
14. D. Gillespie, *Nano Lett.*, 2012, **12**, 1410-1416.
15. H. B. Hu, J. Wen, L. Y. Bao, L. B. Jia, D. Song, B. W. Song, G. Pan, M. Scaraggi, D. Dini, Q. J. Xue and F. Zhou, *Sci Adv*, 2017, **3**, e1603288.
16. J. P. Rothstein, *Annu Rev Fluid Mech*, 2010, **42**, 89-109.
17. T. A. Ho, L. J. Criscenti and Y. F. Wang, *Sci. Rep.*, 2016, **6**, 28053.
18. T. A. Ho, Y. Wang and L. J. Criscenti, *Phys. Chem. Chem. Phys.*, 2018, **20**, 12390-12395.
19. T. A. Ho, Y. Wang, Y. Xiong and L. J. Criscenti, *Fuel*, 2018, **220**, 1-7.
20. X. Gu, D. F. R. Mildner, D. R. Cole, G. Rother, R. Slingerland and S. L. Brantley, *Energ Fuel*, 2016, **30**, 4438-4449.
21. L. F. Ruppert, R. Sakurovs, T. P. Blach, L. L. He, Y. B. Melnichenko, D. F. R. Mildner and L. Alcantar-Lopez, *Energ Fuel*, 2013, **27**, 772-779.
22. P. Ungerer, J. Collell and M. Yiannourakou, *Energ Fuel*, 2015, **29**, 91-105.
23. F. P. Wang and R. M. Reed, *SPE*, 2009, **124253**.
24. R. Qiao, *Microfluid. Nanofluid.*, 2007, **3**, 33-38.
25. A. Q. Shen, Y. K. Liu, X. H. Qiu, Y. J. Lu and S. Liang, *Appl. Phys. Lett.*, 2017, **110**, 121601
26. A. M. J. Edwards, R. Ledesma-Aguilar, M. I. Newton, C. V. Brown and G. McHale, *Sci Adv*, 2016, **2**, e1600183.
27. P. Chiquet, D. Broseta and S. Thibeau, *Geofluids*, 2007, **7**, 112-122.
28. S. Iglauer, *Acc. Chem. Res.*, 2017, **50**, 1134-1142.
29. S. Nakaoka, Y. Yamaguchi, T. Omori, M. Kagawa, T. Nakajima and H. Fujimura, *Phys. Rev. E*, 2015, **92**.
30. C. L. Wang, B. H. Wen, Y. S. Tu, R. Z. Wan and H. P. Fang, *J. Phys. Chem. C*, 2015, **119**, 11679-11684.
31. L. Bocquet and J. L. Barrat, *Phys. Rev. E*, 1994, **49**, 3079-3092.
32. A. B. D. Cassie and S. Baxter, *Trans. Faraday Society*, 1944, **40**, 0546-0550.
33. Y. Y. Liu and J. Wilcox, *Environ. Sci. Technol.*, 2013, **47**, 95-101.
34. Q. Y. Ren, G. J. Chen, W. Yan and T. M. Guo, *J. Chem. Eng. Data*, 2000, **45**, 610-612.
35. S. Khosharay and F. Varaminian, *Int J Refrig*, 2014, **47**, 26-35.
36. Y. L. Liu, H. A. Li and R. Okuno, *Ind Eng Chem Res*, 2016, **55**, 12358-12375.
37. J. Marti, G. Nagy, E. Guardia and M. C. Gordillo, *J. Phys. Chem. B*, 2006, **110**, 23987-23994.
38. S. Senapati and A. Chandra, *J. Phys. Chem. B*, 2001, **105**, 5106-5109.
39. T. Takei, K. Mukasa, M. Kofuji, M. Fuji, T. Watanabe, M. Chikazawa and T. Kanazawa, *Colloid Polym Sci*, 2000, **278**, 475-480.
40. S. Le Caer, S. Pin, S. Esnouf, Q. Raffy, J. P. Renault, J. B. Brubach, G. Creff and P. Roy, *Phys. Chem. Chem. Phys.*, 2011, **13**, 17658-17666.
41. X. F. Huang, Q. Wang, X. X. Liu, S. H. Yang, C. X. Li, G. Sun, L. Q. Pan and K. Q. Lu, *J. Phys. Chem. C*, 2009, **113**, 18768-18771.
42. Y. Hu, D. Devegowda, A. Striolo, A. Phan, T. A. Ho, F. Civan and R. F. Sigal, 2014, **20**, SPE-167234-PA.
43. C. M. Tenney and R. T. Cygan, *Environ. Sci. Technol.*, 2014, **48**, 2035-2042.

TOC

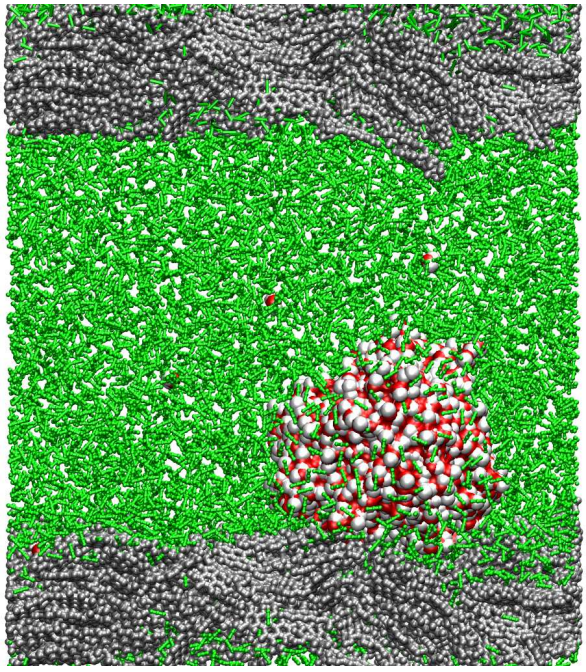

Flow enhancement in rough hydrophilic nanochannel due to an atomistic lubricant